Research Article

Permanent Magnet Synchronous Motor Dynamic Modeling with State Observer-based Parameter Estimation for AC Servomotor Drive Application

Songklod Sriprang*
GREEN-ENSEM, 2 Avenue de la foret de haye, BP 90161Vandoeuvre-les-Nancy, Lorraine, France
Renewable Energy Research Centre (RERC), Thai-French Innovation Institute (TFII)
Department of Teacher Training in Electrical Engineering, Faculty of Technical Education, King Mongkut's University of Technology North Bangkok, Bangkok, Thailand

Babak Nahid-Mobarakeh and Noureddine Takorabet
GREEN-ENSEM, 2 Avenue de la foret de haye, BP 90161Vandoeuvre-les-Nancy, Lorraine, France

Serge Pierfederici
LEMTA-ENSEM, 2 Avenue de la foret de haye, BP 90161Vandoeuvre-les-Nancy, Lorraine, France

Nicu Bizon
Faculty of Electronics, Communications and Computers, University of Pitesti, Arges 110040, Pitesti, Romania

Poom Kuman
Department of Mathematics, Faculty of Science, King Mongkut's University of Technology Thonburi, Bangkok, Thailand

Phatiphat Thounthong
Department of Teacher Training in Electrical Engineering, Faculty of Technical Education, King Mongkut's University of Technology North Bangkok, Bangkok, Thailand

* Corresponding author. E-mail: songklod.sriprang@univ-lorraine.fr DOI: 10.14416/j.asep.2019.11.001
Received: 6 June 2019; Revised: 27 August 2019; Accepted: 23 September 2019; Published online: 8 November 2019

Abstract
This paper presents model-based control with parameters identifies based on extended Luenberger observer of PMSM drive. To control the permanent magnet synchronous motor for high-performance operation, it is still challenging due to its nonlinear properties and unknown parameters. Therefore, to deal with this issue, nonlinear control with parametric identification can offer high-performance control. Both simulations by MATLAB/SIMULINK software and the laboratory experiments were carried out in this research. Simulation and experimental results with a small-scale SPMSM of 6-pole, 1-kW, and 3000 rpm in a laboratory corroborate the control scheme capability during a motor-driven cycle.

Keywords: SPMSM, Extended Luenberger Observer (ELO), and Model-based control

Please cite this article as: S. Sriprang, B. Nahid-Mobarakeh, N. Takorabet, S. Pierfederici, N. Bizon, P. Kuman, and P. Thounthong, "Permanent magnet synchronous motor dynamic modeling with state observer-based parameter estimation for AC servomotor drive application," *Applied Science and Engineering Progress*, vol. 12, no. 4, pp. 286–297, Oct.–Dec. 2019.

1 Introduction

Permanent Magnet Synchronous Motor (PMSM) is popularly used in AC servo drives applications more than other motor types due to the significant advantages such as high power ratio, small volume, and simple structure. These applications require both the rapid electrical response and exact knowledge of the uncertainty disturbance torque as well as the system losses to provide a good transient performance for the system. However, rapid dynamic control of a PMSM is not easy owing to the nonlinearities of PMSM, parameters variation, external disturbance torque, unmodeled uncertainties, etc., which can seriously degrade the performance quality of the motor-driven systems. Thus, the linear control schemes such as proportional–integral control cannot assure required performances. To get around this problem, many researchers have proposed diverse control design methods, e.g., adaptive control [1], neural network control [2], nonlinear feedback linearization control [3], disturbance-observer-based control [4], model predictive control [5], fuzzy-logic-based controller [6], robust control [7] and the combination of these concepts [8]. Recently, several researchers such as [9] and [10] have proposed PMSM control design methods based on the flatness properties of the system called "flatness-based control", which provides a convenient framework for controlling and dealing with nonlinearities or uncertainties. The advantages of flatness-based control are the system's trajectories are straightforwardly estimated by the flat output trajectories and its derivatives without integrating any differential equation.

In this paper, a controller design method using flatness-based control is proposed. And also in order to improve the performance of the control system, machine's parameters including systems losses and external disturbance are going to be estimated by extended Luenberger observer.

In the following sections, a detailed theoretical assay of the proposed method is presented, and simulation results by using MATLAB/Simulink program are provided to prove its effectiveness. Lastly, practical implementation results based on the dSPACE 1104 DSP system are shown to corroborate its correctness.

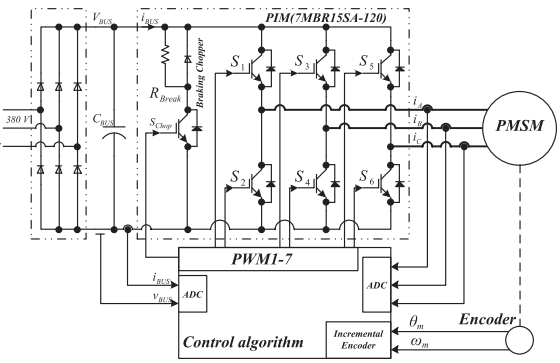

Figure 1: A three-phase inverter driving the PMSM.

2 Propose Modeling and Controller Design

2.1 *Mathematics model of the PMSM/inverter*

Figure 1 shows a system configuration of a three-phase inverter connected to the PMSM. The sinusoidal pulse-width modulation technique (SPWM) is applied to DC-AC inverter to achieve a sinusoidal output voltage with minimal undesired harmonics. The classic rotating reference frame equations of the non-salient PMSM, which define inductances $L_s = L_d = L_q$, are [9]–[12] [Equations (1) and (5)]:

$$\frac{di_d}{dt} = \frac{1}{L_s}(v_d - R_s \cdot i_d - \omega_e \cdot L_s \cdot i_q) \tag{1}$$

$$\frac{di_q}{dt} = \frac{1}{L_s}(v_q - R_s \cdot i_q - \omega_e \cdot L_s \cdot i_d + \Psi_m) \tag{2}$$

$$\frac{d\omega_m}{dt} = \frac{1}{J}(T_e - B_f \omega_m - T_L) \tag{3}$$

where

$$T_e = n_p \cdot \Psi_m \cdot i_q \tag{4}$$

$$\omega_e = n_p \cdot \omega_m \tag{5}$$

v_d and v_q are the d, q-axis voltages, i_d and i_q are the d-, q-axis stator currents, R_s and Ψ_m are the resistance (or system losses) and permanent magnet flux linkage, respectively; and ω_e, ω_m, n_p, T_e, T_L, B_f, J are electrical angular frequency, mechanical angular frequency, number of pole pairs, electromagnetic torque, load torque, viscosity, and inertia, respectively.

2.2 *Flatness-based control design*

Block diagram of all the control algorithm shows in Figure 2 consisted of two main parts, which are the flatness-based control and state observer. Initially, flatness-based control analyzing is described by considering PMSM model and defining $L_s = L_q = L_d$ for non-salient machine. Flat output candidate y, control variable u, and state variable x are defined that $y = [y_1\ y_2\ y_3]^T = [i_d\ i_q\ \omega_m]^T$, u = $[u_1\ u_2\ u_3]^T = [v_d\ v_q\ T_e]^T$, and $x = [x_1\ x_2\ x_3]^T = [i_d\ i_q\ \omega_m]^T$, respectively. To prove that PMSM model is said to be differentially flat, the control variable u has to be written as a function of the flat output and their successive derivative [inverse dynamic] that is [Equations (6) and (7)]

$$u_1 = L_s \cdot \frac{di_d}{dt} + R_s \cdot i_d - \omega_e \cdot L_s \cdot i_q = \psi_1(y_1, \dot{y}_1, y_2) \quad (6)$$

$$u_2 = L_s \frac{di_q}{dt} + R_s \cdot i_q + \omega_e \cdot (L_s \cdot i_d + \Psi_m) = \psi_2(\dot{y}_2, y_2, y_1) \quad (7)$$

By referring to Equation (4), the developed torque equation is proportional to q-axis current that is [Equation (8)]

$$T_e = K_t \cdot i_q \quad (8)$$

where

K_t is defined as the torque constant that $K_t = n_p \cdot \Psi_m$.

Therefore, the T_e is chosen as a control variable $u_3 = T_e = K_t \cdot i_q$. To prove that the system Equation (3) is said to be differentially flat, the input (control) variable u_3 is written as a function of the flat output and its successive derivative (inverse dynamic) that is [Equation (9)]

$$u_3 = \left(J \cdot \frac{d\omega_m}{dt} + T_L + B_f \cdot \omega_m \right) / K_t = \psi_3(y_3, \dot{y}_3) = i_{qCOM} \quad (9)$$

2.3 *Control law and stability*

If all the parameters of the machine are completely known, flatness-based control won't use any controller, but in practice, those are varied all the time by external disturbance. Therefore, the controller has to be discussed to deal with this. Initially, the controller law can defined as follow [Equation (10)]:

$$\lambda = u_{REF} + u_{feedback}(\varepsilon) \quad (10)$$

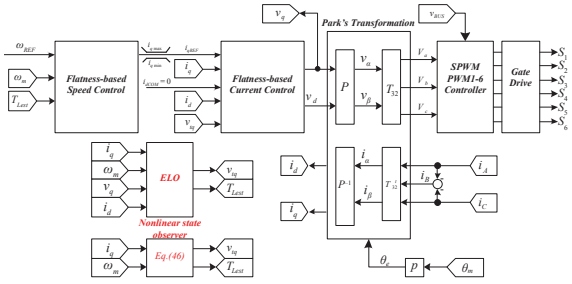

Figure 2: Structure of the PMSM drive system with the flatness-based control and ELO.

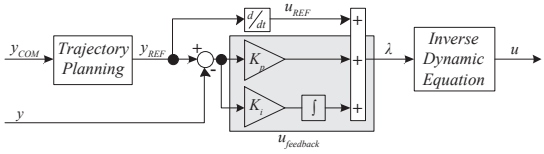

Figure 3: Control law block diagram.

where

ε is an error between y_{ref} and ymeas, $\varepsilon = y_{ref} - y_{meas}$.

λ is the control law output.

Figure 3 shows block diagram of control law for flatness-based control.

As shown in Figure 3, the intelligent proportional-integral controller (iPI) [13] is utilized to compensate an error between reference and measured value. By doing that, the two equations of current loop are defined as follows:

$$\lambda_1 = R_s \cdot \varepsilon_1 + L_s \cdot \frac{d\varepsilon_1}{dt} + K_{p1} \cdot \varepsilon_1 + \int K_{i1} \cdot \varepsilon_1 dt \quad (11)$$

$$\lambda_2 = R_s \cdot \varepsilon_2 + L_s \cdot \frac{d\varepsilon_2}{dt} + K_{p2} \cdot \varepsilon_2 + \int K_{i2} \cdot \varepsilon_2 dt \quad (12)$$

where

ε_1 is an error between y_{1REF} and y_1, $\varepsilon_1 = y_{1REF} - y_1$.

ε_2 is an error between y_{2REF} and y_2, $\varepsilon_2 = y_{2REF} - y_2$.

K_{p1}, K_{i1}, K_{p2}, and K_{i2} are controller parameters.

If the controller is satisfy designed, Equations (11) and (12) will converge to zero that is

$$(R_s + K_{p1}) \cdot \varepsilon_1 + L_s \cdot \frac{d\varepsilon_1}{dt} + \int K_{i1} \cdot \varepsilon_1 dt = 0 \quad (13)$$

$$(R_s + K_{p2}) \cdot \varepsilon_2 + L_s \cdot \frac{d\varepsilon_2}{dt} + \int K_{i2} \cdot \varepsilon_2 dt = 0 \quad (14)$$

Controller parameters can be found out by taking the time-derivative of the Equations (13) and (14) expressed as follows:

$$\ddot{\varepsilon}_1 + \left(\frac{R_s + K_{p1}}{L_s}\right)\cdot\dot{\varepsilon}_1 + K_{i1}\cdot\varepsilon_1 = 0 \quad (15)$$

$$\ddot{\varepsilon}_2 + \left(\frac{R_s + K_{p2}}{L_s}\right)\cdot\dot{\varepsilon}_2 + K_{i2}\cdot\varepsilon_2 = 0 \quad (16)$$

After that, by comparing Equations (15) and (16) to 2nd order system standard equation, controller parameters will obtain as follows [Equation (17)] :

$$\ddot{q}_1 + 2\zeta\omega_{n1}\dot{q}_1 + \omega_{n1}^2 q_1 = 0 \quad (17)$$

Consequently, controller parameters obtained are [Equations (18) and (19)]

$$K_{p1} = K_{p1} = 2\zeta_1\omega_{n1}\cdot L_s - R_s \quad (18)$$

$$K_{i2} = K_{i2} = \omega_{n1}^2 - L_s \quad (19)$$

where
ζ_1 and ω_1 are the desired dominant damping ratio and natural frequency, respectively.

Next, the controller of speed loop control is

$$\lambda_3 = \left(J\cdot\frac{d\varepsilon_3}{dt} + T_L + B_f\cdot\varepsilon_3 + K_{p3}\cdot\varepsilon_3 + \int K_{i3}\cdot\varepsilon_3 dt\right)/K_t \quad (20)$$

where
ε_3 is an error between y_{3REF} and y3, $\varepsilon_3 = y_{3REF} - y3$.
K_{p3}, and K_{i3} are controller parameters.

If the controller is satisfy designed, Equation (20) is going to converge to zero that is

$$J\cdot\frac{d\varepsilon_3}{dt} + T_L + (B_f + K_{p3})\cdot\varepsilon_3 + \int K_{i3}\cdot\varepsilon_3 dt = 0 \quad (21)$$

Taking the time-derivative of the Equation (21) yields

$$\ddot{\varepsilon}_3 + \left(\frac{B_f + K_{p3}}{J}\right)\cdot\dot{\varepsilon} + K_{i3}\cdot\varepsilon_3 = 0 \quad (22)$$

Comparing Equation (22) to second-order system standard equation obtains [Equation (23)]

$$\ddot{q}_2 + 2\zeta\omega_{n2}\cdot\dot{q}_2 + \omega_{n2}^2\cdot q_2 = 0 \quad (23)$$

Consequently, controller parameters obtained are [Equations (24) and (25)]

$$K_{p1} = 2\zeta_2\omega_{n2}\cdot J - B_f \quad (24)$$

$$K_{i2} = \omega_{n2}^2 - J \quad (25)$$

where
ζ_2 and ω_2 are the desired dominant damping ratio and natural frequency, respectively.

2.4 *Trajectory Planning*

As shown in Figure 3, the trajectory planning is a crucial part of fatness-based control because it helps to improve the input reference y_{REF}. The low-pass 2nd filter utilizes to plan the desired trajectory for the flat output component. It allows limiting the derivative terms. Then, planned trajectories of the reference flat output for current and speed loop control are expressed as follows [Equations (26) and (27)]:

$$\frac{y_{1REF}(s)}{y_{1COM}(s)} = \frac{y_{2REF}(s)}{y_{2COM}(s)}\frac{1}{\left(\frac{s}{\omega_{n3}}\right)^2 + \frac{2\zeta_3}{\omega_{n3}}s + 1} \quad (26)$$

$$\frac{y_{3REF}(s)}{y_{3COM}(s)} = \frac{1}{\left(\frac{s}{\omega_{n4}}\right)^2 + \frac{2\zeta_4}{\omega_{n4}}s + 1} \quad (27)$$

where ζ_3, ζ_4, ω_{n3}, and ω_{n4} are the desired dominant damping ratio and natural frequency.

2.5 *Parameters and State Estimation* [14]–[23]

As depicted in Figure 4, there are losses in terms of resistance and switching devices as well as an external disturbance. Besides, owing to the flatness-based control is model-based control; its performance relies on all the parameters of the system. To enhance the system's performance, they have to be estimated by the use of observer approach. The two observer methods are going to introduce and carry out to observe the parameters and state variable of the system. One of them is a linear observer; the other is a nonlinear observer approach.

Initially, extended Luenberger observer is discussed by considering PMSM model. It is due to the non-salient machine that the developed torque is from only the magnetic alignment torque produced by the flux

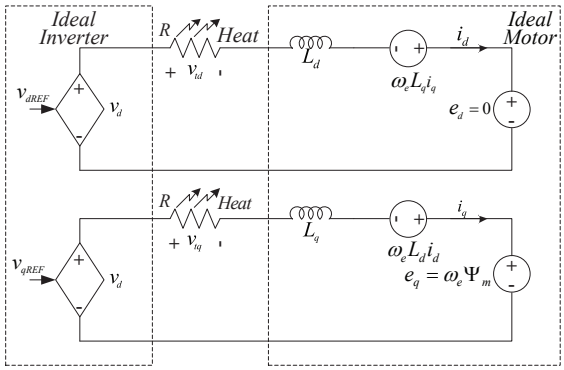

Figure 4: Equivalent of PMSM drive system.

linkage. Therefore, *d*-axis current is set to be zero to reduce copper losses of the machine. Consequently, by neglecting the *d*-axis differential Equation (1) and substituting term $R_s \cdot i_q$ with v_{tq} as well as combining the derivative of torque and v_{tq}, all the system can be rewritten as follows:

$$\frac{di_q}{dt} = \frac{1}{L_s}\left(v_q - v_{tq} - \omega_e \cdot L_s \cdot i_d + \Psi_m\right) \tag{28}$$

$$\frac{d\omega_m}{dt} = \frac{1}{J}\left(T_e - B_f \omega_m - T_L\right) \tag{29}$$

$$\frac{dT_L}{dt} = 0 \tag{30}$$

$$\frac{dv_{tq}}{dt} = 0 \tag{31}$$

dT_L/dt and dv_{tq}/dt can be considered as zero because their time constant is much larger than for a controller. As it a state observer dedicated to the linear system, it is necessary to linearize the considered system around one operating point. Writing the linearization model of PMSM in state-space form yields [Equation (32)]

$$\mathbf{A} = \begin{bmatrix} 0 & -\frac{\Psi_m}{L_s} & -\frac{1}{L_s} & 0 \\ \frac{n_p \cdot \Psi_m}{J} & -\frac{B_f}{J} & 0 & -\frac{1}{J} \\ 0 & 0 & 0 & 0 \\ 0 & 0 & 0 & 0 \end{bmatrix}$$

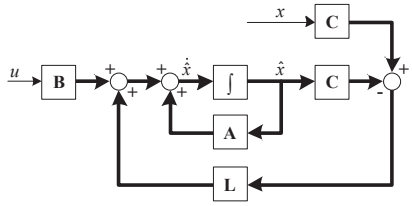

Figure 5: Full-state observer block diagram.

$$\mathbf{B} = \begin{bmatrix} \frac{1}{L_q} & -n_p \cdot \omega_{m0} \\ 0 & 0 \\ 0 & 0 \\ 0 & 0 \end{bmatrix}, \mathbf{C} = \begin{bmatrix} 1 & 0 & 0 & 0 \\ 0 & 1 & 0 & 0 \end{bmatrix} \tag{32}$$

where $x(t) = [i_q \ \omega_m \ v_{tq} \ T_L]^T$, output variables are $y = [i_q \ \omega_m]$ and input variables are $u = [v_q \ i_d]^T$.

According to Luenberger [24], the full-state observer for the system [Equations (33) and (34)]

$$\dot{x}(t) = \mathbf{A}x(t) + \mathbf{B}u(t) \tag{33}$$

$$y(t) = \mathbf{C}x(t) \tag{34}$$

is given by

$$\dot{\hat{x}} = \mathbf{A}\hat{x} + \mathbf{B}u + \mathbf{L}\left(\mathbf{C}x - \mathbf{C}\hat{x}\right) \tag{35}$$

where $\hat{x}$ denotes the estimate of state x.

The observer is depicted in Figure 5. The observer has two inputs, u and y, and one output, $\hat{x}$. The goal of the observer is to provide an estimate $\hat{x}$ so that $\hat{x} \to x$ as $t \to \infty$. Define the observer estimation error as [Equation (36)]

$$e(t) = x(t) - \hat{x}(t) \tag{36}$$

One the main results of the systems theory is that if the system is completely observable, the matrix **L** can be always fined so that the tracking error is asymptotical stable, as desired.

Taking the time-derivative of the estimation error in Equation (37) yields

$$\dot{e} = \dot{x} - \dot{\hat{x}} \tag{37}$$

and using the system model and the observer in Equation (35), it obtains [Equations (38) and (39)]

$$\dot{e} = \mathbf{A}x + \mathbf{B}u - \mathbf{A}\hat{x} - \mathbf{B}u - \mathbf{L}\left(\mathbf{C}x - \mathbf{C}\hat{x}\right) \tag{38}$$

or

$$\dot{e}(t) = \left(\mathbf{A} - \mathbf{LC}\right) \cdot e(t) \tag{39}$$

It is evident that $e(t) \to 0$ as $t \to \infty$ for initial tracking error e(t0) if the characteristic equation

$$\det\left(\lambda\mathbf{I} - \left(\mathbf{A} - \mathbf{LC}\right)\right) = 0 \tag{40}$$

has all its roots in the left haft-plane. Therefore, the observer design process reduces to finding the matrix **L** such that the roots of the characteristic equation in Equation (40) lie in the left haft-plan. This con always be accomplished if the system is completely observable; that is, if the observability matrix $\mathbf{P}_0$ has full rank. [Equation (41)]

$$\mathbf{P}_0 = \begin{bmatrix} \mathbf{C} \\ \mathbf{CA} \end{bmatrix} \tag{41}$$

According to Equation (31), the estimated error $e(t) = \hat{x}(t) - x(t)$ tends to zero if the observer gain **L** is satisfying designed. Then to achieve this, the eigenvalues of [**A-LC**] was established at $[-10000 \; -10000 \; -18 \; -30]^T$. Those values have been tuned experimentally to obtain the better performances as possible. For the operating point, at speed (n) = 1500 rpm ω_{m0} = 157.0796 rad/sec, and $i_{d(0)} = 0$, the matrix **L** is obtained by Equation (42). For this estimation, even if the system has been linearized around one operating point, it has been experimentally verified that the estimation was converging in the speed range 0–1500 rpm with no change of the value of the matrix **L**. The closed-loop system pole locations can be arbitrarily placed if and only if the system is controllable [Equation (42)].

$$\mathbf{L} = \begin{bmatrix} 260 & -18.811 \\ 395.357 & 230.9174 \\ -423.720 & 0 \\ 0 & -11.088 \end{bmatrix} \tag{42}$$

Next, a new observer is introduced to compare to the extended Luenberger observer. It can adapt to the considered problematic consisting of parametric estimation. There was a previous publication that utilized this method to estimate the losses of the boost converter [23]. The proposed state observer is devoted to the subclass of nonlinear systems which can be described as follows:

$$\begin{cases} \dot{\mathbf{X}} = \begin{pmatrix} \dot{x} \\ \dot{d} \end{pmatrix} = \begin{pmatrix} f(x,u) + g(x,u) \cdot d \\ 0 \end{pmatrix} \\ \mathbf{Y} = x \end{cases} \tag{43}$$

where:

1) $\dot{\mathbf{X}} \in \mathbb{R}^{n*m}$ is the vector of the variable which is going to be estimated, and $Y \in \mathbb{R}^{n*m}$ is the vector of measured variable;

2) $x \in \mathbb{R}^n$ is the vector of the system state variable. Every state variable is supposed to be measured (i.e., $\mathbf{Y} = x$);

3) $d \in \mathbb{R}^m$ is the vector of unknown parameters to estimate. Variable d is supposed to very slowly compared to state variables x;

4) f and g are nonlinear functions of x and u (the command signal vector), respectively, of size $\mathbb{R}^n$ and $\mathbb{R}^{n*m}$

Defining state variable x, unknown parameters d, f, and g, respectively that is $x = [i_q \; \omega_m]^T$ and $d = [v_{tq} \; T_L]^T$ from Equations (28)–(31) into Equation (43) yields [Equations (44) and (45)] [25], [26]

$$f(x,u) = \begin{bmatrix} \frac{1}{L_s}\left(v_q - \omega_e \cdot L_s \cdot i_d - \omega_e \cdot \Psi_m\right) \\ \frac{1}{j}\left(p \cdot \Psi_m \cdot i_q - B_f \cdot \omega_m\right) \end{bmatrix} \tag{44}$$

$$g(x,u) = \begin{bmatrix} \frac{-1}{L_s} & 0 \\ 0 & \frac{-1}{J} \end{bmatrix} \tag{45}$$

The estimation error of the state and unknown parameters are $e_x = \hat{x} - x$ and $e_d = \hat{d} - d$, state observer definition is defined as follows:

$$\begin{pmatrix} \dot{\hat{x}} \\ \dot{\hat{d}} \end{pmatrix} = \begin{pmatrix} f(x,u) + g(x,u) \cdot \hat{d} - \mathbf{S} \cdot e_x \\ \mathbf{K}_p \cdot \dot{e}_x + \mathbf{K}_i \cdot e_x - g^t(x,u) \cdot e_x \end{pmatrix} \tag{46}$$

with:

$$\mathbf{K}_p = -\mathbf{P}\cdot g^{-1}(x,u) \tag{47}$$

$$\mathbf{K}_i = \mathbf{K}_p\cdot\mathbf{S} \tag{48}$$

S is the positive-definite matrix of size $\mathbb{R}^{n*m}$.
P is the positive-definite matrix of size $\mathbb{R}^{n*m}$.

The proposed state observer has been designed in order to obtain a system for which the exponential stability can be proven. Especially, for the part of the system corresponding to the estimation of the parameters p—bottom of Equation (46) the term $K_p\cdot\dot{e}_x$ and $K_i\cdot e_x$ have been added so as to verify the exponential stability. Indeed, without those terms (i.e., only considering $\dot{\hat{p}} = -g^T(x,u)\cdot e_x$, only the asymptotic stability can be demonstrated.

For the stability proving of proposed observer, the time-derivative of the estimation error e_x and e_d are written, respectively, as follows:

$$\dot{e}_x = \dot{\hat{x}} - \dot{x} = g(x,u)\cdot e_d - \mathbf{S}\cdot e_x \tag{49}$$

$$\dot{e}_d = \dot{\hat{d}} - \dot{d} = \mathbf{K}_p\cdot g(x,u)\cdot e_d - \mathbf{K}_p\cdot\mathbf{S}\cdot e_x + \mathbf{K}_i\cdot e_x - g^t(x,u)\cdot e_x \tag{50}$$

The exponential stability of the estimation is represented with the classical Lyapunov approach. The candidate function, V is defined by

$$V = \frac{1}{2}\cdot\begin{pmatrix} e_x & e_d\end{pmatrix}\cdot\begin{pmatrix} e_x \\ e_d\end{pmatrix} \geq 0 \tag{51}$$

Taking the time-derivative of the Equation (51) yields

$$\dot{V} = e_x^t\cdot\dot{e}_x + e_d^t\cdot\dot{e}_d \tag{52}$$

By substituting Equations (49) and (50) into Equation (52), $\dot{V}$ can be expressed as [Equation (53)]

$$\begin{aligned}\dot{V} &= e_x^t\cdot g(x,u)\cdot e_d - e_x^t\cdot\mathbf{S}\cdot e_x \\ &+ e_d^t\cdot\mathbf{K}_p\cdot g(x,u)\cdot e_d - e_d^t\cdot\mathbf{K}_p\cdot\mathbf{S}\cdot e_x \\ &+ e_d^t\cdot\mathbf{K}_i\cdot e_x - e_d^t\cdot g^t(x,u)\cdot e_x\end{aligned} \tag{53}$$

Consequently, By referring to Equations (47) and (48), it yields

$$\dot{V} = \frac{1}{2}\cdot\begin{pmatrix} e_x & e_d\end{pmatrix}\cdot\begin{pmatrix} -\mathbf{S} & 0 \\ 0 & -\mathbf{P}\end{pmatrix}\cdot\begin{pmatrix} e_x \\ e_d\end{pmatrix} \tag{54}$$

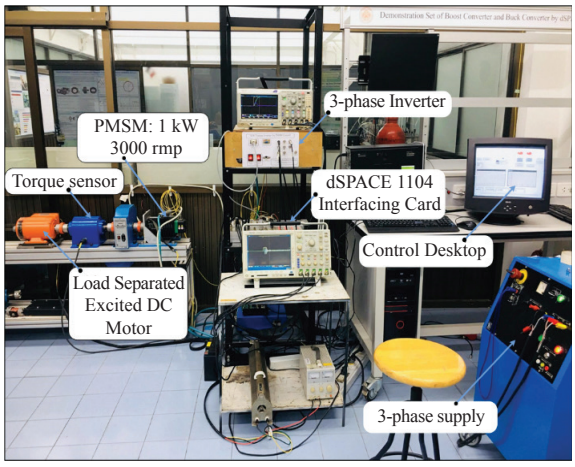

Figure 6: Test bench setup PMSM's drive system.

From Equations (51) and (54), the exponentially stability of the estimation is satisfied long as constant matrix **S** and **P** are positive-definite matrix.

Finally, the constant matrix **S** and **P** have to be tuned by the assumption that the dynamics response of the state error e_x is highly faster than the error of the unknown parameters e_d. Consequently, the constant matrix **S** with eigenvalues real parts is greater than **P**. The experimental tuning is carried out to assure that the convergence of the state error to zero.

3 Simulation and Experimental Validate

3.1 *Laboratory setup*

The main PMSM parameters are presented in Table 1, and the flatness controller parameters are defined in Table 2. The laboratory setup showing in Figure 6 composed of a 6-pole, 1-kW PMSM coupled with a 0.25-kW Separate Excited DC motor that was served as a power supply for a purely resistive load. The stator windings of the PMSM were fed by a 3-kW, 3Φ DC–AC voltage-source inverter (VSI) that was operated at a switching frequency of 10 kHz. The input voltage is obtained through diode rectifier as shown in Figure 1. The drive system was also equipped with an incremental encoder mounted on the rotor shaft and has a resolution of 4096 lines/revolution. The measurement of the electromagnetic torque was realized by a torque transducer mounted on the rotor shaft.

Table 1: PMSM/Inverter and parameters

Symbol	Meaning	Value
T_{rated}	Torque Rated	3 Nm
p	Number of Poles pair	3
R_s	Resistance (Motor + Inverter)	10.1 Ω
$L=L_d=L_q$	Stator inductance	35.31 mH
ψ_m	Magnetic flux	0.2214 Wb
J	Equivalent inertia	0.0022 kg.m^2
B	Viscous friction coefficient	3.5 × 10^{-3} Nm.s/rad
v_{BUS}	DC Bus voltage	530 V
f_s	Switching frequency	10×10^3 Hz

Table 2: Control parameters

Heading 1	Heading 2	Heading 3
ζ_1	Damping ratio 1	1 pu.
ω_{n1}	Natural frequency 1	3200 Rad.s^{-1}
ζ_2	Damping ratio 2	1 pu.
ω_{n2}	Natural frequency 2	320 Rad.s^{-1}
ζ_3	Damping ratio 3	0.7 pu.
ω_{n3}	Natural frequency 3	32 Rad.s^{-1}
ζ_4	Damping ratio 4	0.7 pu.
ω_{n4}	Natural frequency 4	32 Rad.s^{-1}
i_{qmax}	The max. quadrature current	+6 A
i_{qmin}	The min. quadrature current	–6 A

3.2 *Performance of speed acceleration*

Figure 7 depicts the experimental results of speed acceleration response at light load condition (friction losses), n_{COM} 0–1500 rpm and i_{dCOM} = 0 A. It is important to mention that the motor speed is able to track approximately 100% the command. During the acceleration period, the q-axis i_q equals the motor maximum capability ($i_{qmax.}$= +6 A). This ensures that the PMSM runs up in the shortest time possible, and subsequently, the current i_q decreases in order to satisfy the small friction torque.

3.3 *Performance of state variables estimation*

To validate that the controller is appropriately designed, a simulation of the controller was developed using MATLAB/SIMULINK software. Figure 8(a) and (b) show the simulation and experimental results respectively of T_L estimation by using extended Luenberger observer. In Figure 8(a) and (b), Ch1 is the

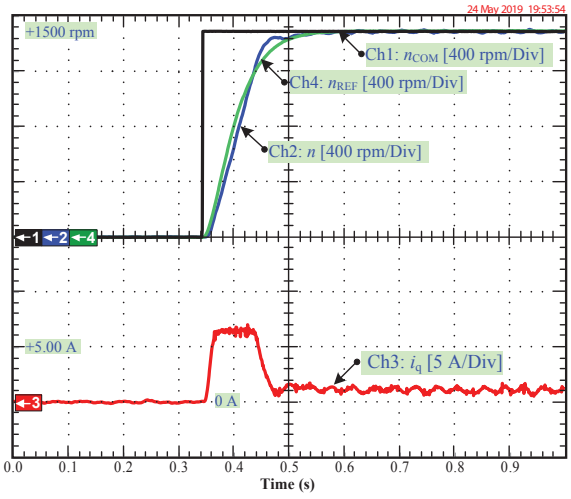

(a)

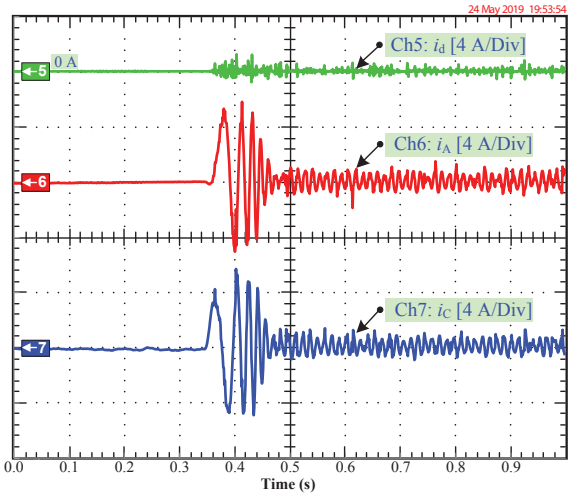

(b)

Figure 7: Experimental result of speed acceleration.

torque reference T_{LREF}, Ch2 is the measured speed n, Ch3 is the q-axis current i_q, and Ch4 is the estimated torque T_{Lest}. The simulation and preliminary results indicate that both are corresponding. The results reflect that when the external disturbance torque is suddenly set from 0 nm to 2 nm, it can be correctly estimated by ELO, and the converging time is less than 0.1 s.

Figure 9(a) shows the simulation results and Figure 9(b) shows the experimental results, respectively of external torque load by using the new observer. In Figure 9(a) and (b), Ch1 is the torque reference T_{LREF}, Ch2 is the measured speed n, Ch3 is the q-axis current

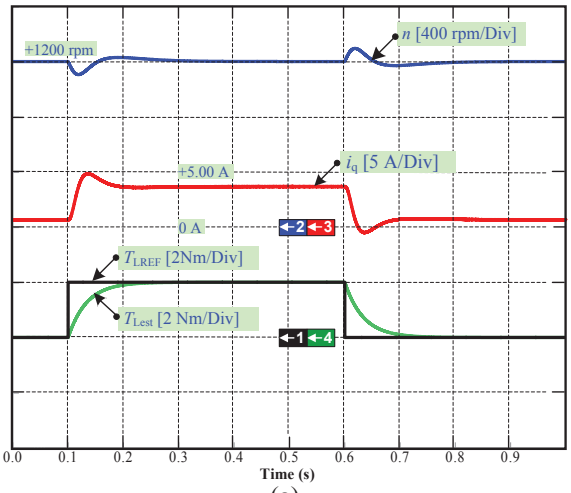

(a)

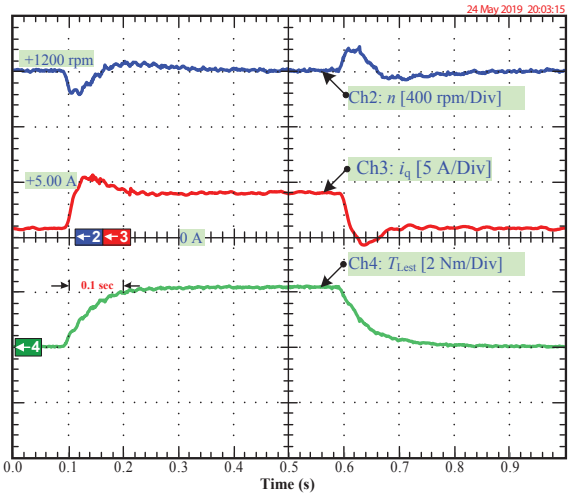

(b)

Figure 8: Simulation and experimental results: External torque load estimation response by using ELO.

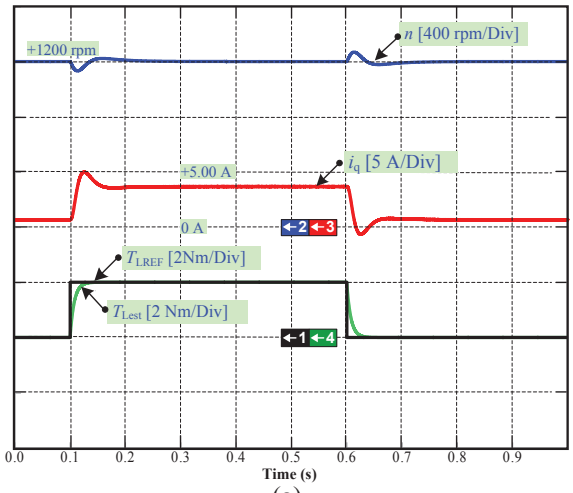

(a)

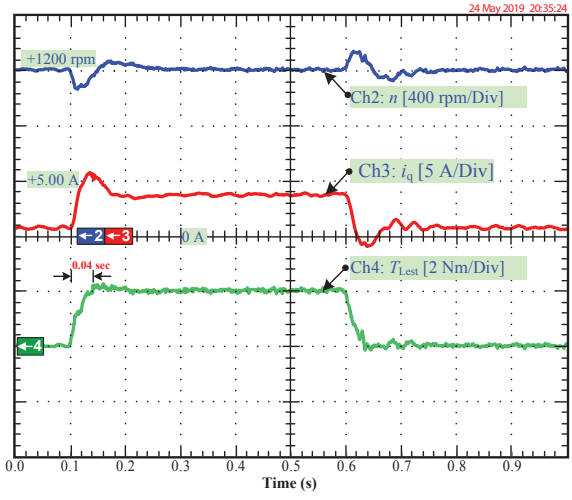

(b)

Figure 9: Simulation and experimental results: External torque load estimation by using the new observer.

i_q, and Ch4 is the estimated torque T_{Lest}. The results reflect that when the external disturbance torque is suddenly taken from 0 nm to 2 nm, it can be correctly estimated by the exponentially stable, and the converging time is less than 0.04 s that is distinctly better than ELO.

3.4 *Speed reversal of flatness-based controller*

The experimental results of speed reversal responses of the system are illustrated in Figure 10, where the motor is forced to reverse its direction.

In Figure 10(a), Ch1 is the speed command n_{COM}, Ch2 is the measured speed n, Ch3 is q-axis current i_q, and Ch4 is the speed reference n_{REF}. In Figure 10(b), Ch5 is d-axis current i_d, Ch6 is the phase A current i_A, and Ch7 is the phase C current i_C. The system operates in a regenerative mode until the speed of the rotor will become positive; and thereafter, the system changes to motoring mode until the rotor speed reaches reference value. The experimental results reflect that the speed of PMSM can efficiently be controlled by flatness-based control. During steady-state region, the speed measurement is able to almost 100% track the speed

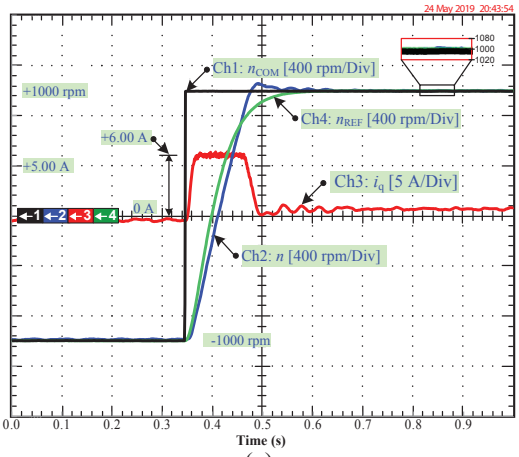

(a)

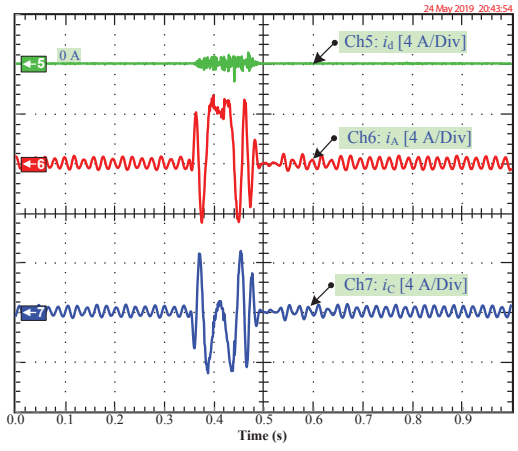

(b)

Figure 10: Experimental results of speed reversal.

reference and the speed command, and q-axis current is restrained without exceeding the current limitation (+6 Ampere).

3.5 *Performance of disturbance rejection*

In Figure 11(a), Ch1 is v_{tq}, Ch2 is the measured speed n, Ch3 is the q-axis iq, and Ch4 is the estimated external torque T_{Lest}. In Figure 11(b), Ch5 is d-axis current i_d, Ch6 is the phase A current i_A, Ch7 is the phase C current i_C. Figure 11(c) shows the trajectories of the transient stator current. To guarantee the stability of the proposed control scheme, the responses of the speed controller and current controller as well as the disturbance rejection ability have been depicted in this section. The new

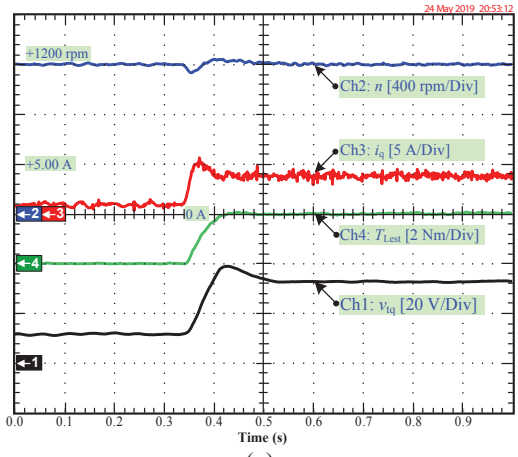

(a)

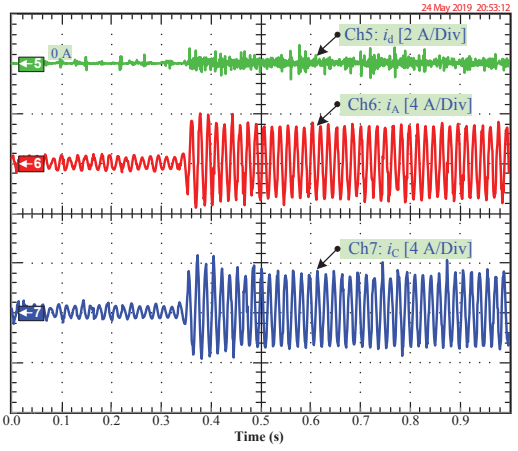

(b)

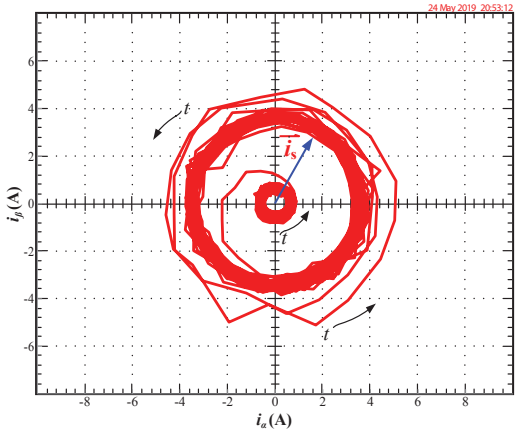

(c)

Figure 11: Experimental results of disturbance rejection.

observer was chosen for estimating the external torque disturbance and the losses of the control system.

The results indicate that when toque command is set to 2 Nm it is able to be satisfyingly estimated by the new observer and v_{tq} is completely observed as well. The reversing time of the speed is lower than 0.1 sec as well as q-axis has a rapid response.

4 Conclusions

This paper presents modeling of permanent magnet motor with parameters identify based on extended Luenberger observer and a new observer method. To control the permanent magnet synchronous motor for high-performance operation, it is still challenging due to its nonlinear properties and unknown parameters. Therefore, to deal with this issue, nonlinear control with parametric identification can offer high-performance control.

Both simulations by MATLAB/SIMULINK software and the laboratory experiments were carried out in this research. A small-scale PMSM was used to validate the proposed control scheme. The simulation and experimental results reflect that flatness-based control can offer the high-performance control of PMSM. Indeed, it provided a satisfying response to both current and speed control. Furthermore, parameters and state variables of the control system were correctly estimated by proposed observer. Moreover, the proposed control scheme can easily be carried out even if with other machines such as induction motor, brushless DC motor, etc.

Acknowledgments

This work was supported in part by the research program in cooperation with the Faculty of Technical Education and the Thai-French Innovation Institute, King Mongkut's University of Technology North Bangkok, with the Universit´e de Lorraine, under Grant KMUTNB-61-GOV-D-68.

Reference

[1] Q. Liu and K. Hameyer, "High-performance adaptive torque control for an IPMSM with real-time MTPA operation," *IEEE Transactions on Energy Conversion*, vol. 32, no. 2, pp. 571–581, 2017.

[2] F. F. M. El-Sousy, "Intelligent optimal recurrent wavelet elman neural network control system for permanent-magnet synchronous motor servo drive," *IEEE Transactions on Industrial Informatics*, vol. 9, no. 4, pp. 1986–2003, 2013.

[3] Y. S. Choi, H. H. Choi, and J. W. Jung, "Feedback linearization direct torque control with reduced torque and flux ripples for IPMSM drives," *IEEE Transactions on Power Electronics*, vol. 31, no. 5, pp. 3728–3737, 2016.

[4] W. H. Chen, J. Yang, L. Guo, and S. Li, "Disturbance-observer-based control and related methods—An overview," *IEEE Transactions on Industrial Electronics*, vol. 63, no. 2, pp. 1083–1095, 2016.

[5] W. Xie, X. Wang, F. Wang, W. Xu, R. M. Kennel, D. Gerling, and R. D. Lorenz, "Finite-control-set model predictive torque control with a deadbeat solution for PMSM drives," *IEEE Transactions on Industrial Electronics*, vol. 62, no. 9, pp. 5402–5410, 2015.

[6] Y. C. Chang, C. H. Chen, Z. C. Zhu, and Y. W. Huang, "Speed control of the surface-mounted permanentmagnet synchronous motor based on Takagi–Sugeno Fuzzy models," *IEEE Transactions on Power Electronics*, vol. 31, no. 9, pp. 6504–6510, 2016.

[7] R. Cai, R. Zheng, M. Liu, and M. Li, "Robust control of PMSM using geometric model reduction and μ-synthesis," *IEEE Transactions on Industrial Electronics*, vol. 65, no. 1, pp. 498–509, 2018.

[8] H. Li, J. Wang, H. K. Lam, Q. Zhou, and H. Du, "Adaptive sliding mode control for interval type-2 fuzzy systems," *IEEE Transactions on Systems, Man, and Cybernetics: Systems*, vol. 46, no. 12, pp. 1654–1663, 2016.

[9] P. Thounthong, B. YODWONG, and S. Sikkabut, "Model based control of permanent magnet AC servo motor drives," presented at the 19th International Conference on Electrical Machines and Systems (ICEMS), Stuttgart, Germany, Nov. 13–16, 2016.

[10] H. Sira-Ramírez, J. Linares-Flores, C. García-Rodríguez, and M. A. Contreras-Ordaz, "On the control of the permanent magnet synchronous motor: An active disturbance rejection control approach," *IEEE Transactions on Control Systems Technology*, vol. 22, no. 5, pp. 2056–2063, 2014.

[11] P. Pillay and R. Krishnan, "Control characteristics and speed controller design for a high performance permanent magnet synchronous motor drive," *IEEE Transactions on Power Electronics*, vol. 5, no. 2, pp. 151–159, 1990.

[12] L. Wang, J. Jatskevich, and H. W. Dommel, "Re-examination of synchronous machine modeling techniques for electromagnetic transient simulations," *IEEE Transactions on Power Systems*, vol. 22, no. 3, pp. 1221–1230, 2007.

[13] N. Matsui, T. Makino, and H. Satoh, "Autocompensation of torque ripple of direct drive motor by torque observer," *IEEE Transactions on Industry Applications*, vol. 29, no. 1, pp. 187–194, 1993.

[14] J. Solsona, M. I. Valla, and C. Muravchik, "Nonlinear control of a permanent magnet synchronous motor with disturbance torque estimation," *IEEE Transactions on Energy Conversion*, vol. 15, no. 2, pp. 163–168, 2000.

[15] Y. A. R. I. Mohamed, "Design and implementation of a robust current-control scheme for a PMSM vector drive with a simple adaptive disturbance observer," *IEEE Transactions on Industrial Electronics*, vol. 54, no. 4, pp. 1981–1988, 2007.

[16] Y. Zhang, C. M. Akujuobi, W. H. Ali, C. L. Tolliver, and L. S. Shieh, "Load disturbance resistance speed controller design for PMSM," *IEEE Transactions on Industrial Electronics*, vol. 53, no. 4, pp. 1198–1208, 2006.

[17] M. Yang, X. Lang, J. Long, and D. Xu, "Flux immunity robust predictive current control with incremental model and extended state observer for PMSM drive," *IEEE Transactions on Power Electronics*, vol. 32, no. 12, pp. 9267–9279, 2017.

[18] W. Deng, C. Xia, Y. Yan, Q. Geng, and T. Shi, "Online multiparameter identification of surface-mounted PMSM considering inverter disturbance voltage," *IEEE Transactions on Energy Conversion*, vol. 32, no. 1, pp. 202–212, 2017.

[19] S. Diao, D. Diallo, Z. Makni, C. Marchand, and J. F. Bisson, "A differential algebraic estimator for sensorless permanent-magnet synchronous machine drive," *IEEE Transactions on Energy Conversion*, vol. 30, no. 1, pp. 82–89, 2015.

[20] F. Tinazzi and M. Zigliotto, "Torque estimation in high-efficency IPM synchronous motor drives," *IEEE Transactions on Energy Conversion*, vol. 30, no. 3, pp. 983–990, 2015.

[21] Y. Sangsefidi, S. Ziaeinejad, A. Mehrizi-Sani, H. Pairodin-Nabi, and A. Shoulaie, "Estimation of stator resistance in direct torque control synchronous motor drives," *IEEE Transactions on Energy Conversion*, vol. 30, no. 2, pp. 626–634, 2015.

[22] G. Wang, L. Ding, Z. Li, J. Xu, G. Zhang, H. Zhan, R. Ni, and D. Xu, "Enhanced position observer using second-order generalized integrator for sensorless interior permanent magnet synchronous motor drives," *IEEE Transactions on Energy Conversion*, vol. 29, no. 2, pp. 486–495, 2014.

[23] H. Renaudineau, J. P. Martin, B. Nahid-Mobarakeh, and S. Pierfederici, "DC–DC converters dynamic modeling with state observer-based parameter estimation," *IEEE Transactions on Power Electronics*, vol. 30, no. 6, pp. 3356–3363, 2015.

[24] R. C. Dorf and R. H. Bishop, *Modern Control Systems*, 12th ed., London, UK: Pearson Education, 2011, pp. 847–850.

[25] M.-A. Shamsi-Nejad, B. Nahid-Mobarakeh, S. Pierfederici, and F. Meibody-Tabar, "Fault tolerant and minimum loss control of doublestar synchronous machines under open phase conditions," *IEEE Transactions on Industrial Electronics*, vol. 55, no. 5, pp. 1956–1965, 2008.

[26] M. Shamsi-Nejad, B. Nahid-Mobarakeh, S. Pierfederici, and F. Meibody-Tabar, "Fault tolerant permanent magnet drives: Operating under open-circuit and shortcircuit switch faults," *KMUTNB Int J Appl Sci Technol*, vol. 7, no. 1, pp. 57–64, 2014.